Marine Structures 83 (2022) 103145

Contents lists available at ScienceDirect

Marine Structures

journal homepage: www.elsevier.com/locate/marstruc

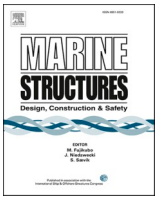

Analysis of spar and semi-submersible floating wind concepts with respect to human exposure to motion during maintenance operations

Mert Kaptan [a], Bjørn Skaare [a,b,*], Zhiyu Jiang [c], Muk Chen Ong [a]

[a] Department of Mechanical and Structural Engineering and Materials Science, University of Stavanger, Stavanger, Norway
[b] Equinor ASA, Stavanger, Norway
[c] Department of Engineering Sciences, University of Agder, Grimstad, Norway

ARTICLE INFO

Keywords:
Offshore wind
Floating platforms
Response amplitude operator
Seasickness
Workability

ABSTRACT

Floating offshore wind turbines (FOWTs) are expected to experience onsite maintenances and inspections during their lifetimes. To carry out offshore maintenance activities, a crew will be transferred to an FOWT and spend several hours on board. A challenge may arise if the motions of a floating platform affect the crew's comfort level and further jeopardise their work performance or even health. To address this challenge, this paper analyses the motion characteristics and dynamic properties of a spar and two semi-submersible FOWTs, all exhibiting very different motion characteristics. The impact of the platform motions and accelerations on the workability of the FOWTs are investigated. We carry out hydrodynamic analysis in a potential-flow software for the FOWTs and estimate the relevant short-term root-mean-square values for relevant motions and accelerations of the parked FOWTs in the frequency domain. Hindcast data for two representative sites in Norway and South Korea are selected, and both single peaked and double peaked wave spectra are considered. Using the limiting motion response criteria from a NORDFORSK study, we calculate the workability index of the FOWTs for the two locations. It is found that both the spar and the semi-submersible floating wind concepts fulfil the limiting criteria for significant wave heights up to the maximum known significant wave height for crew transfers to FOWTs. The present study contributes to a better understanding of FOWTs during the maintenance phase.

1. Introduction

A water depth of 60 m is considered as a cut-off level for bottom-fixed structures and the entry point of the floating platforms in the offshore wind industry due to economic reasons [1]. According to Musial [1], almost 80% of the world's offshore wind resource potential is currently profitable only for floating offshore wind turbines (FOWTs).

Some of the floating platform concepts such as spar buoys, semi-submersibles and tension-leg-platforms are well-proven concepts after years of successful operation in the oil and gas industry [2]. Spar buoys are ballast-stabilised simple structures with inherently high stability with a large draft which decreases their deployments in relatively shallow waters. Semi-submersibles are complex free-surface stabilised structures with a relatively small draft which provides high site flexibility. Tension leg platforms are mooring

* Corresponding author. Equinor ASA, Stavanger, Norway.
E-mail address: bjorn.skaare@uis.no (B. Skaare).

https://doi.org/10.1016/j.marstruc.2021.103145
Received 9 June 2021; Received in revised form 3 October 2021; Accepted 20 November 2021
Available online 1 February 2022

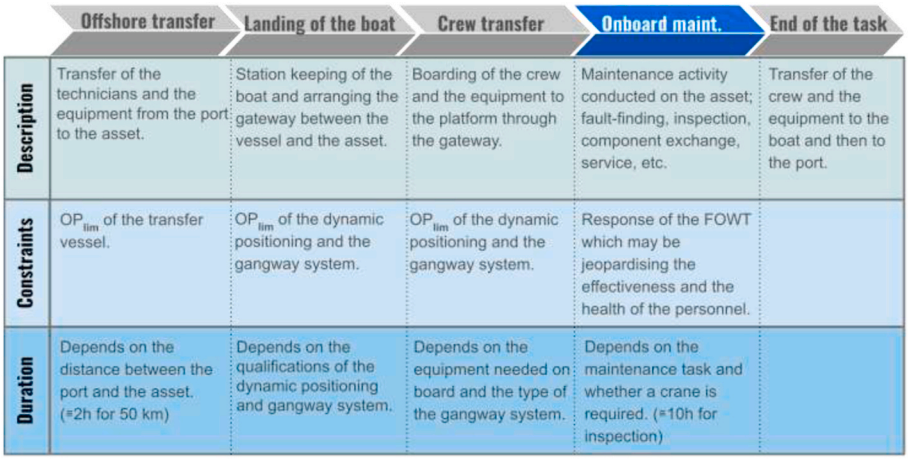

Fig. 1. Flow chart with the different stages of a regular maintenance activity performed on an FOWT from start (left) to the end (right) with the descriptions (top), constraints (middle) and approximate durations (bottom) of each stage. The focus of this study; onboard maintenance (blue) is highlighted. (For interpretation of the references to color in this figure legend, the reader is referred to the Web version of this article.)

line-stabilised structures with low weight that are potentially sensitive to the mooring and anchoring systems and involve a complex installation.

The 2.3 MW spar buoy concept Hywind Demo was the first full-scale FOWT in the world when installed off the West coast of Norway in 2009 [3], while the 2 MW WindFloat 1 was the first full-scale semi-submersible wind turbine when installed off the coast of Portugal in 2011 [4]. Among the 15 floating wind turbines that are currently in operation in the world [5], the floating foundations include eight spar buoys, five semi-submersibles and two barges with damping pool. The floating wind industry is still at an early stage, but a rapid development is expected over the next 5 years. 17 floating wind projects are under development with an overall installed capacity above 2 GW between 2021 and 2026, with semi-submersible floaters as the dominating concept [5].

Operation and maintenance will become increasingly important as floating wind projects move from demonstration and pre-commercial stages to commercial stages. Even though humans are not needed in the operation of FOWTs on a daily basis, they are still required to be on board to perform corrective, condition-based or calendar-based maintenances. By today, access to the offshore wind turbines is conducted with three main transport types; *(i) Crew Transport Vessel (CTV)*, *(ii) Service Operations Vessel (SOV)* and *(iii) Helicopter*, based on the scale of the operation, i.e., how far a platform is located from shore and forecasted sea and weather conditions. CTVs and SOVs are mainly restricted by the sea conditions, while visibility, wind speed and motions of the floater are the main concerns for transportation with a helicopter. SOVs are larger and better-equipped vessels compared to CTVs.

Fig. 1 shows that a maintenance operation on an FOWT may be considered as a combined problem of accessibility and maintainability. The operation begins with the transfer of the technicians and required equipment to the platform. It is important to maintain the well-being of the personnel onboard during the transfer. Therefore, most vessels are equipped with individual suspension seats to minimise the travel fatigue and stress caused by the vessel motion [6]. After arrival at the platform, the vessel must be station-kept and a safe access between the vessel and the platform needs to be maintained. For that purpose, some vessels are equipped with station-keeping systems such as dynamic positioning or a gripping system which improves access to the turbine ladder [7]. Motion compensated gangway systems are often applied to provide safe access to the platform. Access to the platform is mainly constrained by the sea conditions and relevant operational limits of the transfer vehicle and the equipment used in this operation while the duration is related with the distance to the platform and the vessel and equipment properties. Operational limits (OP_{lim}) of the some SOVs may reach up to significant wave height H_s of 4.5 m while gangways usually operate in H_s below 3 m. For further information about the operational limits of the commercial transfer vessels, gangways and dynamic positioning systems, reader is referred to reference [6]. However, this study particularly focuses on the maintainability of the FOWTs and maintenance activity conducted onboard with its constraints.

Besides accessibility, maintainability of FOWTs is also important to avoid longer downtime, rescheduling of the maintenance operation and potential extra operation and maintenance costs. The maintainability of FOWTs is also dependent on the workability of maintenance personnel. When it is considered that a typical workday offshore counts 12 h which approximately consists of 10 h spent on the platform and 2 h spent on the transfer vessel, comfort and effectiveness of the maintenance personnel onboard the FOWT becomes an important matter to finish the maintenance activity within a pre-decided weather window [8]. Therefore, motion characteristics of the FOWTs and the exposure of maintenance personnel to their motions are important to achieve high maintainability for the asset.

Motions of FOWTs may be considered as a vibration signal to investigate the exposure of the maintenance personnel. The signal could be defined by its measured amplitude throughout a period or amplitude of vibration versus the frequency spectrum of the source which is the floater in this case. Based on the frequency range of the excitation vibration and its effect on humans, human exposure to vibration may be categorised under two categories [9]. The first category is called whole-body vibration, which defines the vibration

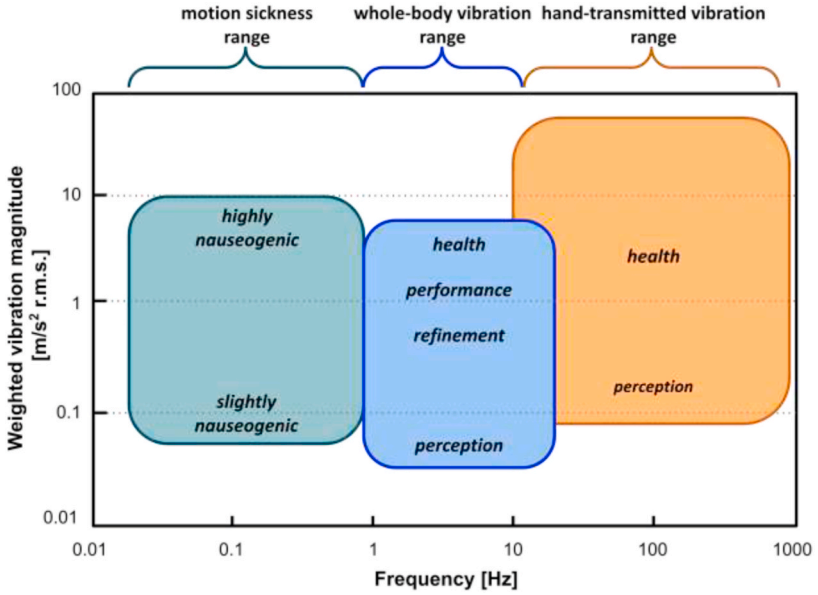

Fig. 2. Typical frequency ranges and magnitudes of interest for the study of motion sickness (green), whole body vibration (blue), and hand-transmitted vibration (orange). (For interpretation of the references to color in this figure legend, the reader is referred to the Web version of this article.)

within a frequency range from 0.5 to 80 Hz that affects the whole body. It is common to experience such vibration while travelling in a car, bus, train etc. On the other hand, the second category is referred to as hand-arm vibration, which expresses the vibration that affects only the part of the body in contact with the vibration source, typically in a frequency range of 6.5–1250 Hz. This type of vibration may be experienced while using a drilling machine or while driving a car by transmitting from the device to the human body through hands and arms. An FOWT will typically be in parked condition during maintenance activities and the dynamic response is dominated by wave excitations. Since both the natural frequencies of FOWTs and the wave frequency range are usually well below 1 Hz, only the whole-body vibration is considered relevant and investigated in this study.

Typical frequency ranges and the symptoms relevant to the magnitude of the vibration has been discussed by Ref. [10] and is illustrated in Fig. 2. Exposure of motion sickness and whole-body vibration for a certain time could cause health problems that would endanger the health and safety of the maintenance personnel during their work on the platform, such as dizziness, nausea and vision loss [9]. Sufficient magnitude of hand-transmitted vibration could also cause health issues such as muscle and joint disorders if it occurs long enough [10]. However, this study particularly focuses on the motions of FOWT and their possible effects on the personnel.

The frequency range and amplitude of the vibration are not the most ideal way to evaluate human exposure to vibration considering the complexity of the human body. Accordingly, most international standards define the limit of human exposure to vibration in terms of root mean square (RMS) values of motions of the excitation source, which is the floating platform in this case.

Human exposure to motion during maintenance of floating offshore wind turbines is previously studied [8] by response analyses in the time domain for four different floater concepts. In the study, spar, semi-submersible, barge and tension leg platform concepts were simulated with load cases generated from metocean parameters based on the design loading conditions at different locations. The concept of using a workability index as a measure for the workable time relative to all available time below a given significant wave height was introduced based on relevant motion and acceleration limiting criteria from the NORDFORSK study [11]. The workability index was calculated for all four floater concepts, but the results for the different concepts were anonymised.

The purpose of this paper is to analyse and compare the inherent dynamic properties of two of the dominant FOWT concepts – the spar buoy and the semi-submersible – with respect to important parameters for human exposure, such as floater pitch motion, horizontal and vertical acceleration at both the platform and nacelle level, where maintenance work is carried out. Further, analyses are carried out in the frequency domain to compare.

- The responses relevant for human exposure based on generic sea states using both the JONSWAP (Joint North Sea Wave Project) [12] and Torsethaugen wave spectra [13].
- The workability index for two relevant locations for future deployment of floating wind – one location at the coast of Norway and one location at the coast of South Korea - based on random load cases from hindcast data with good correlation with the long-term distributions for waves and directions and using both the JONSWAP and Torsethaugen wave spectra.

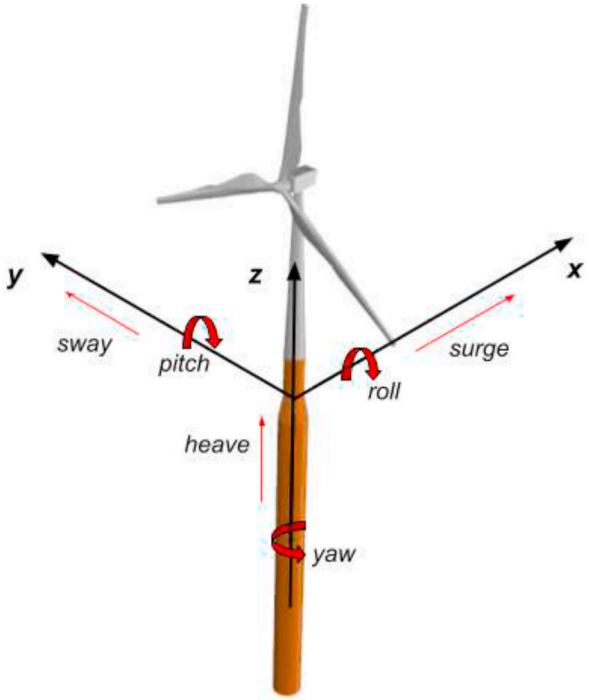

Fig. 3. Body-fixed coordinate system for FOWT and degrees of freedom.

2. Methodology

The methodology developed for numerical study of the human comfort for FOWTs is given in this section. First, the frequency-domain approach is presented including the assumptions made and modelling/simulation tools used. Second, short-term statistics is provided for estimating the floater responses in irregular sea conditions, followed by the sets of load cases that are generated from the hindcast data of two sites relevant to FOWT deployment. Then, the derivation and choice of adequate limiting motion criterion regarding the exposure of humans to vibration is explained. Last, the definition and calculation of the workability index is presented.

2.1. Frequency-domain approach

During offshore access and maintenance operations, FOWTs are typically parked, and their motions in mild and moderate wave conditions during maintenance activities are mainly caused by the wave-induced rigid body motion of the platform [14]. The wind loads are significantly reduced when an FOWT is in parked conditions and the generator torque is zero. It is further assumed that a feasible tower design implies that the first flexible bending frequency of the tower and substructure is sufficiently above the wave frequency range. Thus, a linear force-motion relation can be implied, and the frequency-domain approach can be applied to quickly estimate the short-term response statistics based on statistical assumptions. Hence, the structural flexibilities are ignored and the system transfer function is linearised.

For a floating platform, the body-fixed, right-handed cartesian coordinate system is illustrated in Fig. 3. The system origin is at the still water level, with the positive z-direction pointing upwards. The six degrees of freedom (DOFs) shown in the figure are of interest in this study.

For a floating body with six DOFs, the equation of motion can be presented as follows

$$(\boldsymbol{M}+\mathbf{A})\cdot\ddot{\boldsymbol{x}}+\mathbf{B}\cdot\dot{\boldsymbol{x}}+\boldsymbol{C}\cdot\boldsymbol{x}=\mathbf{F} \tag{1}$$

where $\boldsymbol{M}$ is the system mass matrix, $\boldsymbol{A}$ and $\boldsymbol{B}$ are the frequency-dependent hydrodynamic added mass and damping matrices, $\boldsymbol{C}$ is the stiffness matrix, and $\boldsymbol{F}$ is the excitation force. The damping matrix $\boldsymbol{B}$ includes both frequency-dependent potential damping and linearised viscous damping. Stochastic linearisation is applied to linearise the viscous damping due to flow separation of the slender elements according to Ref. [15]. The stiffness matrix includes the hydrostatic stiffness and the linearised mooring stiffness.

The solution to Equation (1) is the response amplitude operators (RAOs). To obtain the RAOs of an FOWT, the mass matrices of the systems are obtained by creating finite element models of the whole FOWTs with distributed mass in GeniE [16] followed by establishing the 6 × 6 mass matrix. The hydrodynamic analysis is carried out using a potential-flow solver WADAM [17]. The effects of irregular frequencies are also removed to exclude the spikes of body response caused at the frequencies where artificial sloshing resonance modes inside the body take place [18]. When solving for the RAOs, additional restoring matrices corresponding to the

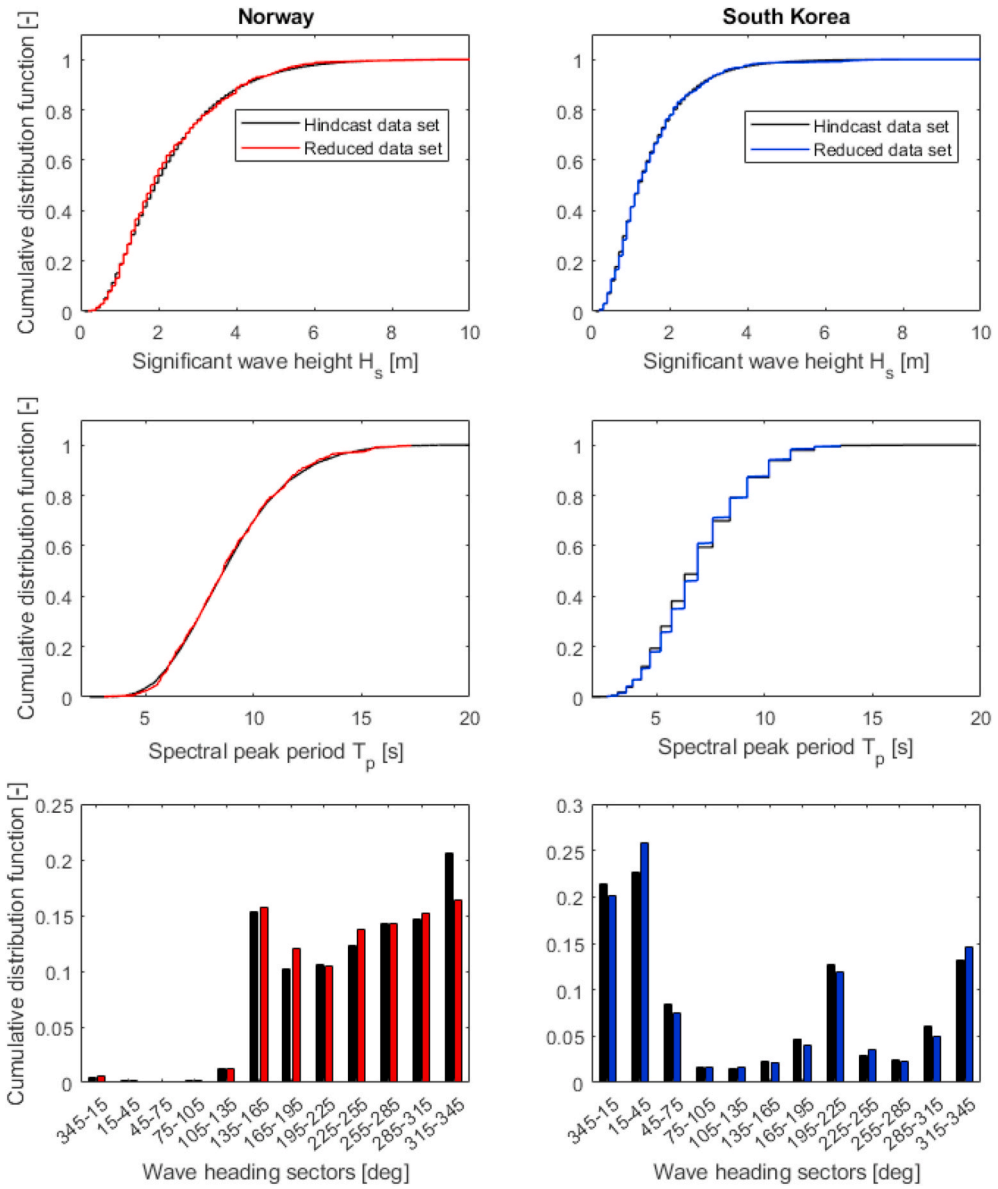

Fig. 4. Comparison of the cumulative distributions of significant wave height (top), the cumulative distribution of spectral peak period (middle), and the distribution of wave heading sectors (bottom). Distributions for Norway (left) with hindcast data set (black) and reduced data set (red). Distributions for South Korea (right) with hindcast data set (black) and reduced data set (blue). (For interpretation of the references to color in this figure legend, the reader is referred to the Web version of this article.)

linearised stiffness of the mooring lines are specified such that the mooring effects are considered. The models are simulated as a set of regular waves within a frequency range from 0 to 0.5 Hz for different headings with an interval of 10° to obtain the RAOs of the floaters as a function of excitation frequency for each heading.

2.2. Short-term statistics

Short-term statistics is applied in this study to estimate the response statistics of the floaters in a sea state for a given reference time. The basic assumption is that each short-term sea state is stationary, and the platform motion responses are Gaussian. Based on the RAOs, statistical values of the responses can be calculated, including the short-term extremes or response standard deviation of the displacement, velocity, and acceleration for a specified point on an FOWT. The 3 h reference time is chosen for the short-term statistics calculation as recommended for simulations of irregular sea states [19,20].

Two different wave spectra are considered to model the sea conditions to observe the sensitivity of the floaters' response with

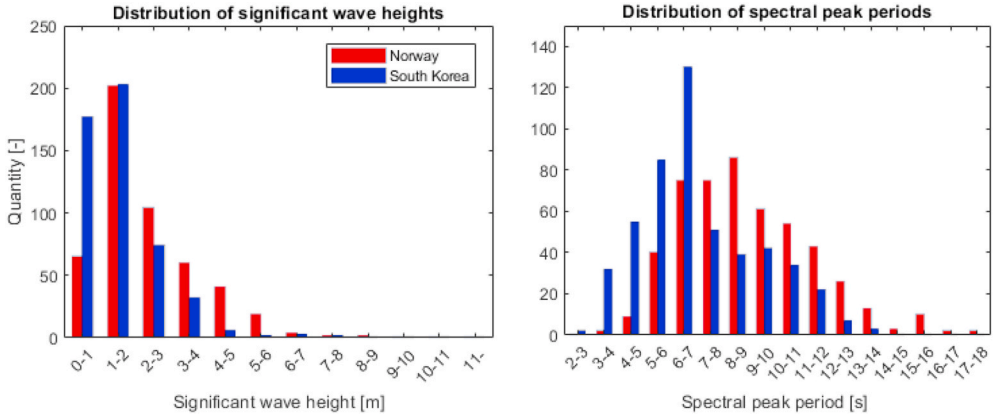

Fig. 5. Distributions of significant wave heights (left) and spectral peak periods (right) from the reduced set of load cases for Norway (red) and South Korea (blue). (For interpretation of the references to color in this figure legend, the reader is referred to the Web version of this article.)

respect to the wave spectral models:

- The JONSWAP which is a modified/peak-enhanced Pierson-Moskowitz spectrum.
- The Torsethaugen wave spectrum which is a 2-peaked spectral model developed for the North Sea.

Each load case is considered a fully developed sea and is modelled separately by the JONSWAP and Torsethaugen spectra. The recommended nondimensional peak shape parameter (γ) and spectral width parameters (σ_a, σ_b), which are derived from experimental data, are used to form the spectral models [18]. The spectral density is calculated for each loading condition as a function of wave frequency.

The RAOs in this study are calculated for the nacelle level (1.7 m, 0 m, 89.6 m) and the platform level (0 m, 0 m, 10.0 m) since these are the locations where maintenance personnel spend the most time during their work. The response spectra for the floaters $R_{ij}(\omega,\beta)$, are calculated for each degree of freedom as a function of wave frequency, ω, and wave heading, β, for each load case as

$$R_{ij}(\omega,\beta) = |\eta_i(\omega,\beta)|^2 \, S_j(\omega), \tag{2}$$

where the index i represents the degree of freedom (surge = 1, sway = 2, heave = 3, roll = 4, pitch = 5, yaw = 6), $\eta_i(\omega,\beta)$ represents the RAO of the relevant mode of the motion in each DOF, and $S_j(\omega,\beta)$ represents the spectral density as a function of wave frequency for load case j. RMS values of the motions for each DOF and sea state are further derived from the relevant response spectrum. RMS motions are derived from the square root of the zeroth moment of the response spectrum, $m_{i,j}$.

$$m_{i,j} = \int_0^{2\pi} \int_0^{\infty} \omega^0 R_{ij}(\omega,\beta) d\omega d\beta \tag{3}$$

$$rms_{ij} = \sqrt{m_{i,j}} \tag{4}$$

2.3. Metocean data

During the maintenance of the FOWTs, the rotor blades are set to a parked position. Therefore, the wind loads are assumed negligible and are not included in this study. Overall significant wave height, spectral peak period, and wave heading are used to model the sea state in each load case in the later simulation study for two selected locations in Norway and South Korea.

A reduced dataset of approximately 500 load cases have been selected with a good representation of the distributions for significant wave height, spectral peak period, and wave heading, from hindcast data for two locations relevant for deployment of floating wind turbines at the coast of Norway and South Korea. The load cases have been selected from 100 000 random draws of approximately 500 load cases from the hindcast database, where the random draw with best correlation with the distributions was selected.

Hindcast data for the South Korean location include 25 years of data that are reduced to 502 load cases, while the hindcast data for the Norwegian location include 40 years of data that are reduced to 501 load cases. The correspondence between the distributions from the hindcast data set and the reduced data set used in this study are shown for both locations in Fig. 4. The good correspondence observed for both locations indicate that the reduced set of load cases should be representative when considering environmental conditions during maintenance operations.

A comparison of the distributions of the significant wave heights and spectral peak periods for the reduced set of load cases used in the analyses for Norway and South Korea are shown in Fig. 5. Harsher wave conditions are observed for the Norwegian location with higher significant wave heights and higher spectral peak periods compared to the South Korean location.

Table 1
Set of criteria with regards to vertical/lateral accelerations and rotational displacement [11].

Description	Vertical acceleration (RMS)	Lateral acceleration (RMS)	Rotational displacement (RMS)
Light manual work[a]	0.20g	0.10g	6.0°
Heavy manual work	0.15g	0.07g	4.0°
Intellectual work[b]	0.10g	0.05g	3.0°
Transit passenger[c]	0.05g	0.04g	2.5°
Cruise liner	0.02g	0.03g	2.0°

[a] Tolerable less than 1 h [22].
[b] 0.5 h exposure for people unused to ship motions [23].
[c] 2 h exposure for people unused to ship motions [23].

Table 2
Main particulars of reference models.

Parameter	OC3-Hywind	CSC-Semisubmersible	WindFloat
Mass	8014 t	10337 t	4640 t
Displacement	8177 t	10503 t	4640 t
Pre-tension at fairlead	163 t	166 t	54.5 t
Location of COG	(0, 0, −78) m	(0,0, −18.9) m	(-0.278, 0.0, 3.728) m
Location of COB	(0, 0, −62.1) m	(0, 0, −22.4) m	(0.426, 0.0, −13.79) m
Draft	120 m	30 m	17 m
Water depth	320 m	200 m	150 m
Surge natural period	125.0 s	76.9 s	108.6 s
Heave natural period	31.3 s	25.6 s	19.9 s
Pitch natural period	29.4 s	31.3 s	43.2 s

2.4. Derivation of limiting sea states

Motion signals that are derived from short-term statistics are evaluated against a set of limiting criteria based on a publication by the Nordic Research Collaboration [11] which is referenced and used in assessment criteria by several researches [8,21,22] regarding exposure of humans to vibration. The threshold levels for rotations, vertical and lateral accelerations are given as root mean square values. The limiting criteria from Ref. [11] based on the type of work that is going to be performed are presented in Table 1.

The maintenance work in the FOWTs, which typically takes 12 h as a combination of 10 h spent on the floater and 2 h spent on the transit vessel, is often demanding and could require accuracy and high concentration of the personnel [8]. The "Intellectual Work'' criterion represents reference values for "half an hour exposure period for people unused to ship motions'' while "Transit Passenger'' stands for a set of reference values for people in the same category but 2 h exposure [24]. Only 2 h do not reflect the real exposure time of the maintenance personnel during their work onboard an FOWT. Still, the "Transit Passenger'' criterion is found the most relevant since it is the longest time frame reference value for "people who are not used to be exposed to vessel motions". "Transit Passenger'' is therefore selected as the limiting criterion in this study, in line with [8].

2.5. Definition of workability index

The concept of a Workability Index (WI) presented by Ref. [8] is also utilised in this study to present the performances of different floaters with respect to exposure of maintenance personnel to motion. RMS values for rotational motion, lateral and vertical accelerations are calculated for each load case and are assessed against the limiting criteria. Load cases with any mode of the RMS motion responses exceeding the corresponding threshold are considered unworkable.

The WI is calculated as a function of the significant wave height, and a subset of load cases is defined for each significant wave height. The WI within each subset can then be defined as

$$WI = \frac{\sum_{j=1}^{m} q_j}{\sum_{i=1}^{n} q_i}, \tag{5}$$

where q_j represents the probability of a workable load case in the subset, m is the number of workable load cases, q_i represents the probability of a load case in the subset, and n is the number of load cases within the subset. The WI within a subset ranges between 0 and 1, where WI = 1 corresponds to 100% workability within the subset.

3. Spar and semi-submersible floating wind concepts

A spar and two different semisubmersible floaters are selected in this study since spars and semisubmersibles are currently the dominating floating offshore wind turbine concepts. The following three well-defined reference models that are all designed to support the NREL 5-MW reference wind turbine [25] are considered in this study:

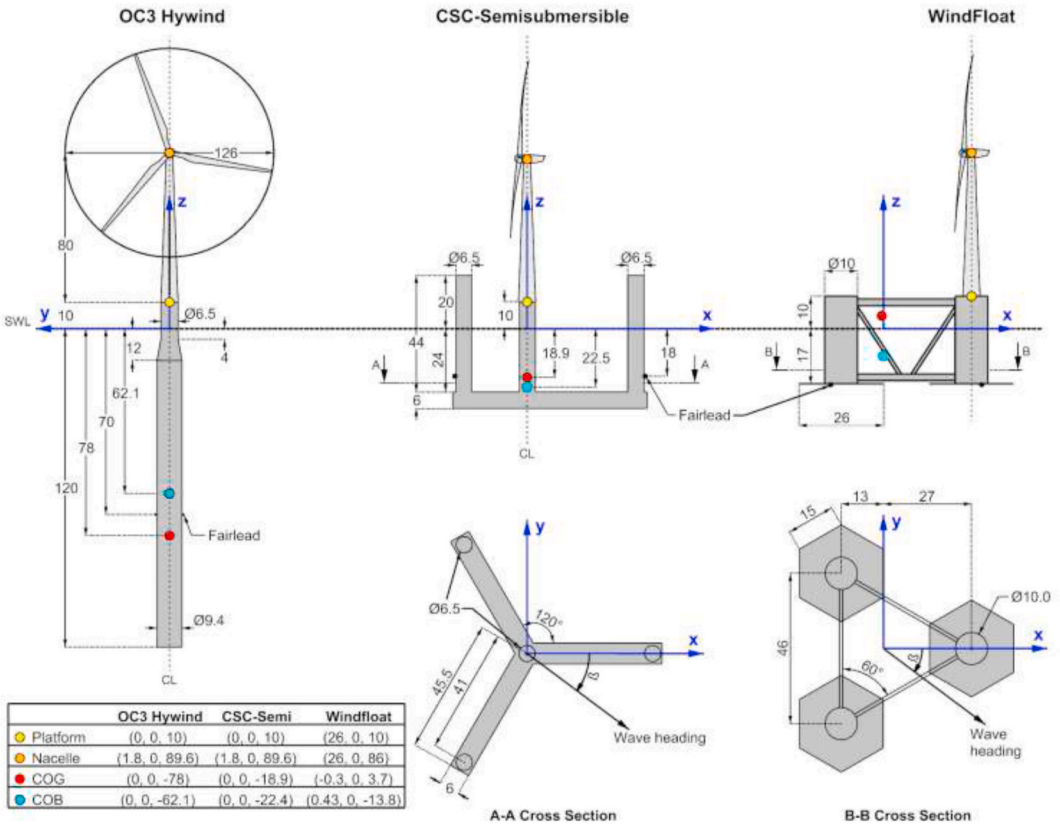

Fig. 6. Geometry of reference models; OC3-Hywind (left), CSC-Semisubmersible (middle) and WindFloat (right). Dimensions are given in meters.

- The OC3-Hywind [26] which was developed for the Offshore Code Comparison Collaboration (OC3) as part of Phase IV.
- The CSC-Semisubmersible [27] that was developed as a reference semi-submersible wind turbine within the Norwegian Research Centre for Offshore Wind Technology (NOWITECH).
- The generic 5 MW WindFloat concept reported in Ref. [28].

All three concepts have been tested in model scale experiments [28–30], while the Hywind and WindFloat concepts have also been deployed in full scale in several projects.

3.1. OC3-hywind, CSC-Semisubmersible and WindFloat

The main particulars of the floating wind turbine concepts are shown in Table 2, with the corresponding geometries shown in Fig. 6. The most protuding differences between the concepts are that.

- The OC-3 Hywind achieves its basic stability from ballasting with its center of gravity (COG) far below the center of buoyancy (COB). Both the CSC-Semisubmersible and WindFloat achieve their basic stability from their well distributed waterplane area. However, it is noted that the vertical distance between the COG and COB are quite different between the two semisubmersibles. The vertical location of the COG is 3.6 m above the COB for CSC-Semisubmersible, while the corresponding distance is 17.5 m for WindFloat.
- The CSC-Semisubmersible has the largest mass, which is 29% larger than OC3-Hywind and 122.8% larger than Windfloat.
- The draft of OC3-Hywind is naturally by far the deepest, but the difference between the two semisubmersible concepts is also significant, with the CSC-Semisubmersible having a 76.5% deeper draft than WindFloat. The deep draft of the CSC-Semisubmersible could make installation from a conventional quay challenging, and thereby losing an important advantage of the semisubmersible type FOWTs.
- The CSC-Semisumersible is a braceless structure with 4 columns where the wind turbine is placed on a center-column, while WindFloat is a semisubmersible with braces with 3 columns where the wind turbine is placed on one of the columns.

Despite the above differences it is seen that the differences in natural period is not that large. All three concepts have natural periods in heave and pitch that are above the typical range of wave periods with heave natural periods ranging between 19.9 s–31.3 s

Fig. 7. Panel models for the FOWT concepts considered: CSC-Semisubmersible (top-left), WindFloat (bottom-left), OC3-Hywind (right).

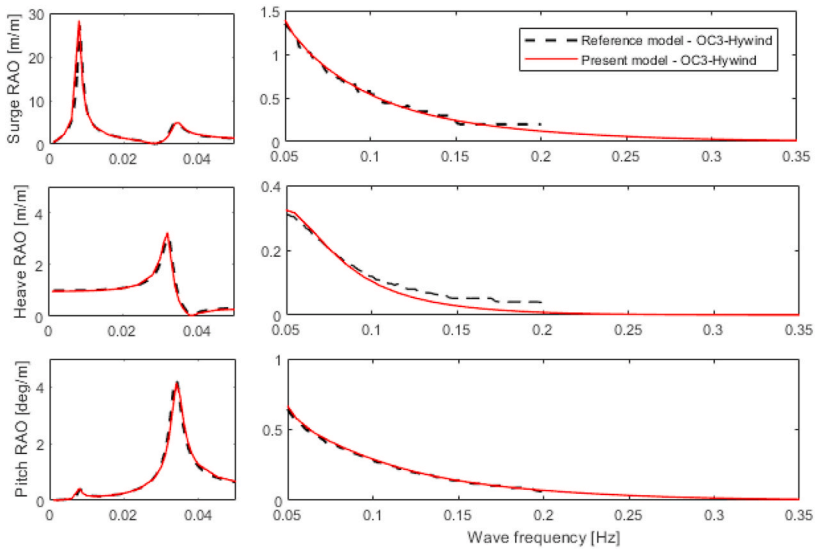

Fig. 8. Surge (top), heave (middle), and pitch (bottom) RAO's for the reference OC3-Hywind model from Ref. [25] (dashed black) and the present OC3-Hywind model (red), that is used in this study when excited by regular waves with 0° wave heading. (For interpretation of the references to color in this figure legend, the reader is referred to the Web version of this article.)

and pitch natural periods ranging between 29.4s–43.2 s.

OC3-Hywind is a slender and cylindrical shaped structure with a deep draft of 120 m. The bottom part of the cylinder is filled with water and fixed ballast to create a positive righting lever when the structure is tilted, by keeping its centre of gravity (COG) lower than the centre of buoyancy (COB). The diameter of the structure is 9.4 m from the keel until 12 m beneath the free surface. The cylinder's diameter is tapered down from 9.4 m to 6.5 m starting from that level. The reduced diameter in the wave zone will reduce the wave loads and the reduced area in the water plane will increase the natural period in heave.

The CSC-Semisubmersible is a braceless hull with a symmetrical shape, but with a more complicated geometry compared to the OC3-Hywind. It consists of one central column and 3 outer columns mounted on 3 pontoons that are aligned with 120° in between. Each column has a diameter of 6.5 m and height of 44 m while the central column is 10 m shorter than the rest. The CSC-Semisubmersible is mainly stabilised by its well-distributed waterplane area and submerged volume that allows COB to shift to the more submerged side and create a positive righting moment when displaced.

The WindFloat is an asymmetric semisubmersible floater with braces between three columns and the wind turbine tower is placed on top of one of the columns. Water entrapment plates are placed on the bottom of the columns to increase the added mass in heave such that the natural period in heave is outside the typical range of wave periods, but also to provide additional damping. Further, an active ballast system transfer water between the columns to keep the platform upright against the wind direction.

All concepts have the connection of the tower structure and the floating platform 10 m above the still water level (SWL). The OC3 Hywind and the CSC-Semisubmersible have a nacelle level at 89.6 m height, while WindFloat has a nacelle level of 86.0 m.

The mooring system for the OC3 Hywind and the CSC-Semisubmersible concepts is composed of three catenary chain mooring lines. WindFloat uses a catenary mooring system with 4 mooring lines, where two of the mooring lines are placed on the column with

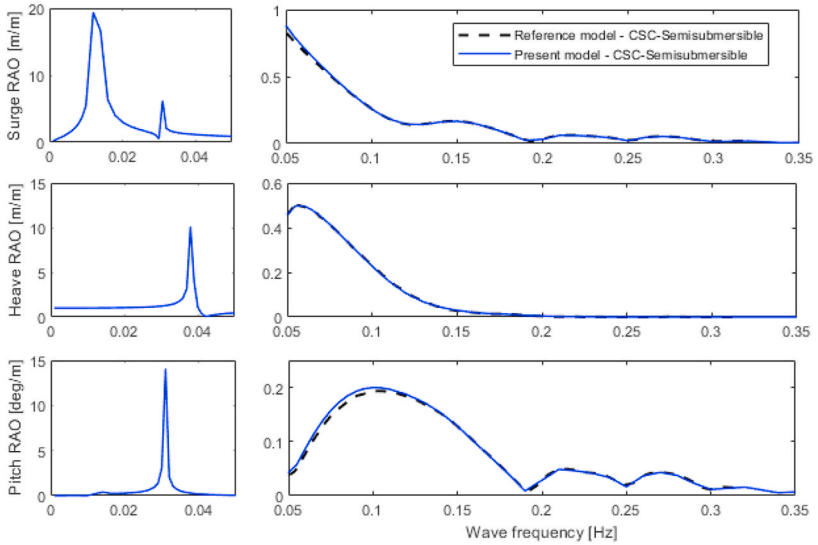

Fig. 9. Surge (top), heave (middle), and pitch (bottom) RAO's for the reference CSC-Semisubmersible model from Ref. [26] (dashed black) and the present CSC-Semisubmersible model that is used in this study (blue), when excited by regular waves with 0° wave heading. (For interpretation of the references to color in this figure legend, the reader is referred to the Web version of this article.)

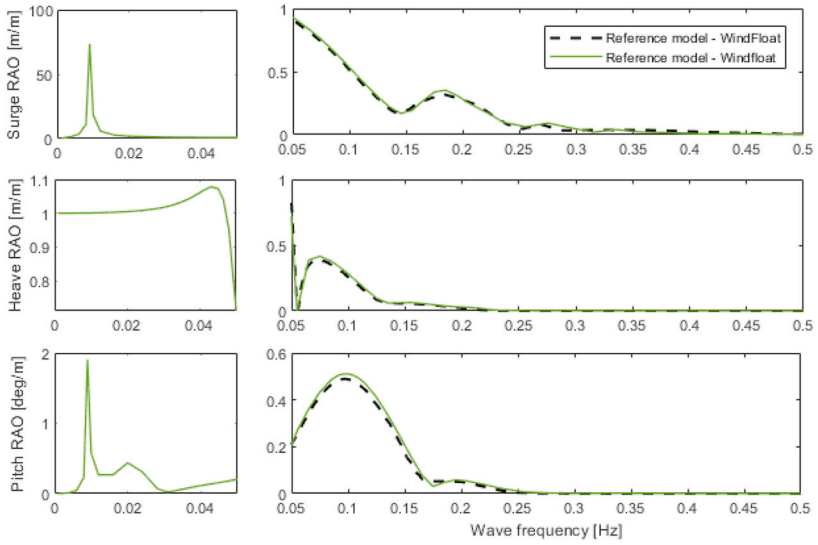

Fig. 10. Surge (top), heave (middle), and pitch (bottom) RAO's for the reference WindFloat model from Ref. [28] (dashed black) and the present WindFloat model that is used in this study (green), when excited by regular waves with 0° wave heading. (For interpretation of the references to color in this figure legend, the reader is referred to the Web version of this article.)

the wind turbine. Each mooring line on WindFloat consists of segments with chain on the top and the bottom with polyester rope in between and includes a clump weight. For all concepts, one end of the mooring line is connected to the fairlead on the floater while the other end is connected to an anchor that is buried under the soil on the seabed.

3.2. Model validations

Three-dimensional panel models are created for the different FOWT concepts as shown in Fig. 7. The OC3-Hywind panel model consists of approximately 4000 rectangular panels while CSC-Semisubmersible's model is formed with approximately 2000 panels. The WindFloat panel model has approximately 9000 panels due to complexity of the geometry. The largest panel size is set to 1×1 m^2 for all models.

To validate the accuracy of the hydrodynamic models developed for this study – denoted as the present models - a frequency

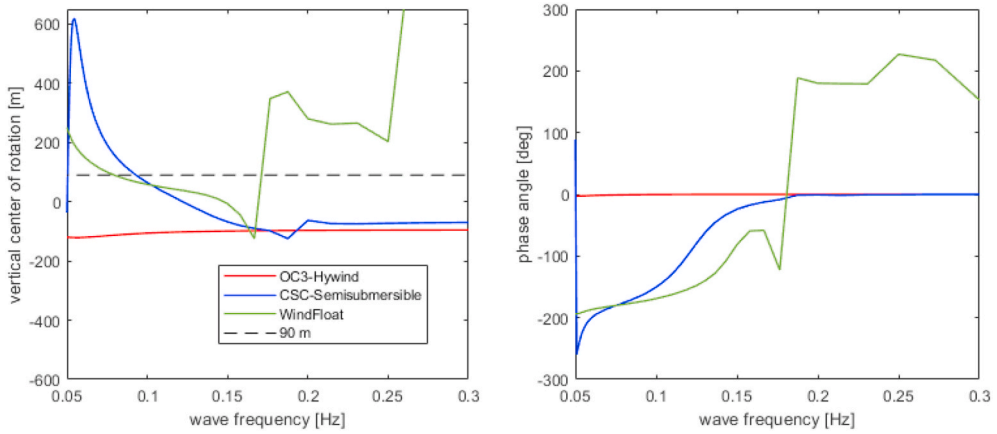

Fig. 11. Vertical position of centre of rotation (left) and phase angle between surge and pitch motion (right) for OC3 Hywind (red), CSC-Semisubmersible (blue), and WindFloat (green). The median nacelle level for the three floaters at 90 m is indicated (dashed black). (For interpretation of the references to color in this figure legend, the reader is referred to the Web version of this article.)

domain response analysis is performed. These results are compared with corresponding results from the original publications of the OC3-Hywind [26], CSC-Semisubmersible [27], and WindFloat [28] – denoted as the reference models. The wind turbine is considered rigid in all models, and only regular waves are considered. Wind and current loads are neglected. Comparison of the RAOs from the present models and reference models are shown for OC3-Hywind, CSC-Semisubmersible and WindFloat in Figs. 8–10.

Generally good agreement is observed between the reference and present models for all concepts and motions considered.

4. Dynamic properties

4.1. Centre of rotation

The vertical centre of rotation of a floating structure can be considered as the frequency dependent vertical position without horizontal motion. The centre of rotation is a useful dynamic property to understand the horizontal motions and accelerations at different vertical locations for different floater designs. Under the assumption of harmonic floater motions in surge, η_1 , heave, η_3 , and pitch, η_5, and generally small pitch angles, the horizontal surge motion at a given vertical position z is given as

$$\eta_{surge}(z) = \eta_1 + z\eta_5, \tag{6}$$

where $\eta_{surge}(z)$ is the surge motion at a vertical position z along the structure. From Equation (6) it is seen that $\eta_{surge}(z) = 0$ is achieved for

$$z = -\frac{\eta_1}{\eta_5} \tag{7}$$

Generally, the complex transfer function $H_i(\omega_j, \beta)$ between wave and motion response i is found as

$$H_i(\omega_j, \beta) = \frac{\eta_i(\omega_j, \beta)}{\zeta_{A_j}}, \tag{8}$$

for a regular wave with frequency ω_j, amplitude ζ_{A_j} and wave heading β . Insertion of Equation (8) into Equation (7) gives the centre of rotation on the form

$$z = \mathrm{Re}\left\{ -\frac{|H_1(\omega_j)|}{|H_5(\omega_j)|} e^{i(\delta_{1j} - \delta_{5j})} \right\}, \tag{9}$$

where δ_{ij} is the phase angle for motion response i at frequency j.

The frequency dependent centre of rotation and the phase angle between surge and pitch motion are shown as function of wave frequency in Fig. 11 for the OC3-Hywind, CSC Semisubmersible and WindFloat. It is seen that the centre of rotation for OC3-Hywind does not change significantly with wave frequency, and that the surge and pitch motion of the OC3-Hywind are in phase for all wave frequencies. This is opposite to both the CSC-Semisubmersible and WindFloat. An advantageous property of both semisubmersible concepts, and WindFloat in particular, is that the centre of rotation is close to the nacelle level at ~90 m for wave frequencies around ~0.1 Hz where the wave energy content is typically high. This gives reduced structural fatigue damage due to wave induced motions at the nacelle in this frequency range. On the other hand, for wave frequencies around ~0.2 Hz, the centre of rotation of both the CSC

Table 3
Combinations of wave directions and wave lengths and corresponding wave periods/frequencies – that are expected to give increased surge loading on the CSC-Semisubmersible due to the floater geometry in the wave zone.

Wave headings [deg]	Wave length [m]	Period [s]	Frequency [Hz]	Description
0, 60, 120, 180, 240, 300	20.5	3.62	0.276	Horizontal wave loads on all 4 columns in phase
0, 60, 120, 180, 240, 300	61.5	6.28	0.159	Horizontal wave loads on 3 outer columns in phase - centre column 120 deg out of phase
0, 60, 120, 180, 240, 300	30.75	4.43	0.225	Horizontal wave loads on 3 outer columns in phase - centre column 240 deg out of phase
30, 90, 150, 210, 270, 330	35.5	4.76	0.210	Horizontal wave loads on all 4 columns in phase
30, 90, 150, 210, 270, 330	17.75	3.37	0.300	Horizontal wave loads on all 4 columns in phase

Table 4
Combinations of wave directions and wave lengths and corresponding wave periods/frequencies – that are expected to give increased surge loading on WindFloat due to the floater geometry in the wave zone.

Wave headings [deg]	Wavelength [m]	Period [s]	Frequency [Hz]	Description
0, 60, 120, 180, 240, 300	39.8	5.05	0.198	Horizontal wave loads on all 3 columns in phase
0, 60, 120, 180, 240, 300	19.9	3.57	0.280	Horizontal wave loads on all 3 columns in phase
0, 60, 120, 180, 240, 300	13.3	2.91	0.343	Horizontal wave loads on all 3 columns in phase
30, 90, 150, 210, 270, 330	46	5.43	0.184	Horizontal wave loads on 2 columns in phase, one column 180 deg out of phase
30, 90, 150, 210, 270, 330	23	3.84	0.261	Horizontal wave loads on all 3 columns in phase

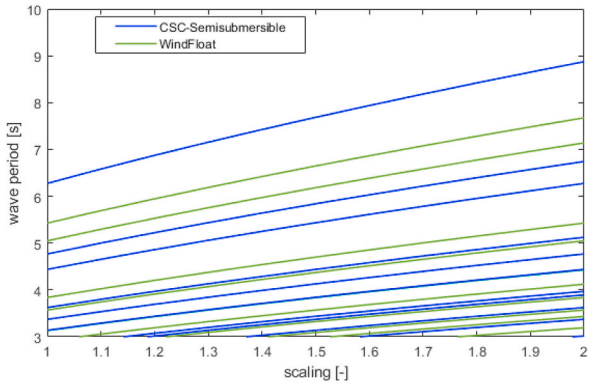

Fig. 12. Effect of scaling on wave periods leading to horizontal wave loads in phase on the columns of CSC-Semisubmersible (blue) and WindFloat (green). (For interpretation of the references to color in this figure legend, the reader is referred to the Web version of this article.)

Semisubmersible and WindFloat are further from the nacelle than for OC3 Hywind. The centre of rotation for WindFloat is above the nacelle level for higher wave frequencies, indicating that the horizontal motion at the platform level is larger than the horizontal motion at the nacelle level in this frequency range.

4.2. Wavelength and geometric properties of the CSC Semisubmersible and WindFloat

The geometry of buoyancy stabilised floaters in the wave zone can cause special peaks in the response spectrum depending on wavelength and wave heading. The surge wave excitation forces will have a peak when the horizontal wave loads on the columns are in phase. Similarly, the pitch wave excitation forces will have a peak when the when the horizontal wave loads on the columns are 180° out of phase. The latter was not found to be of significant influence on the overall surge lateral acceleration response. Therefore, horizontal wave loads on the columns in phase, corresponding wavelengths and headings are considered in the following.

By assuming infinite water depth, the wave period, T, corresponding to a given wavelength, λ, becomes [31]:

$$T = \sqrt{\frac{2\pi\lambda}{g}}, \tag{10}$$

where g is the acceleration of gravity.

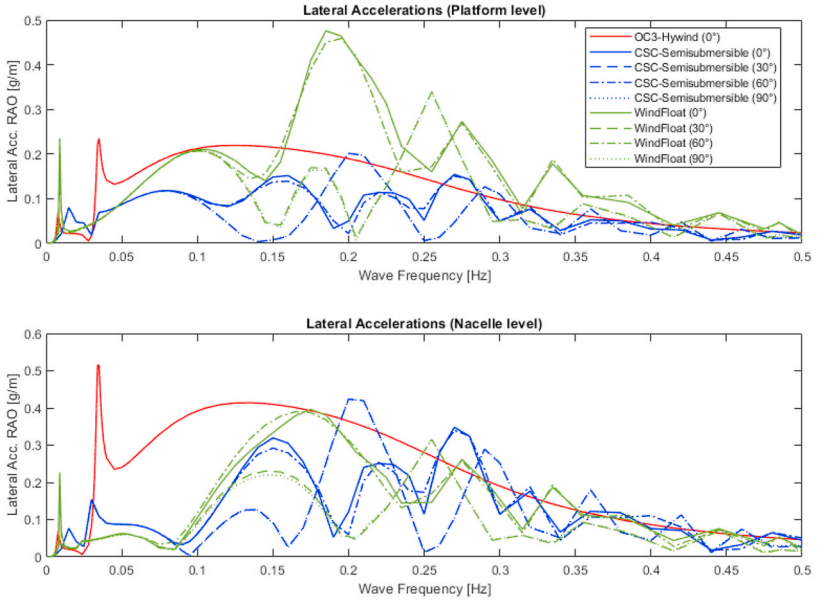

Fig. 13. Lateral acceleration RAOs along the wave heading direction the OC3-Hywind (red), CSC-Semisubmersible (blue), and WindFloat (green) at the platform level (top) and at the nacelle level (bottom). (For interpretation of the references to color in this figure legend, the reader is referred to the Web version of this article.)

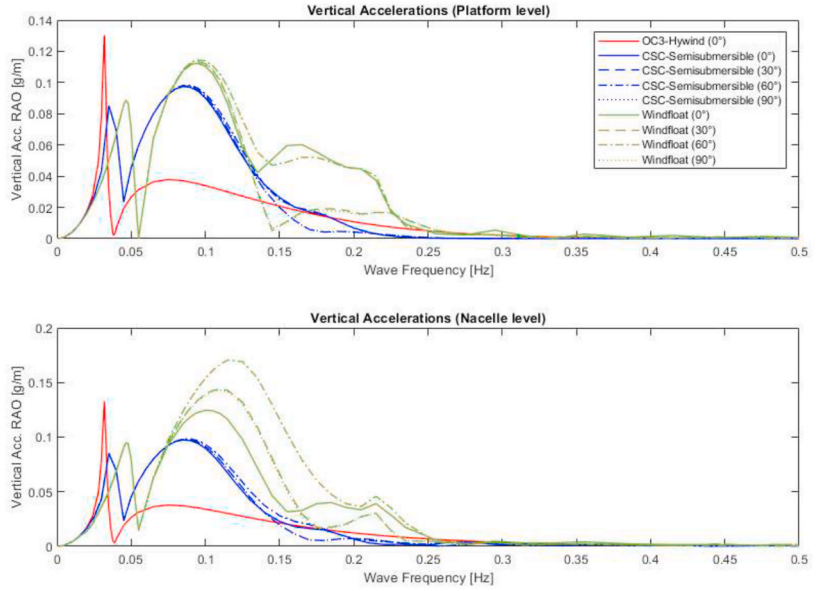

Fig. 14. Vertical acceleration RAOs along the wave heading direction for the OC3-Hywind (red), CSC-Semisubmersible (blue), and WindFloat (green) at the platform level (top) and at the nacelle level (bottom). (For interpretation of the references to color in this figure legend, the reader is referred to the Web version of this article.)

The wave loads on the columns of the CSC-Semisubmersible shown in Fig. 6 are in phase for the combinations of wave headings and wave periods shown in Table 3. Only wavelengths corresponding to wave periods larger than 3.0 s are considered. It is seen that the horizontal wave loads on the columns are in phase for a broad range of wave headings and wave periods.

Similarly, the wave loads on the columns of WindFloat shown in Fig. 6 are in phase for the combinations of wave headings and wave periods shown in Table 4.

There is an extensive growth in the offshore wind industry both in terms of installed capacity and turbine size. Wind turbines with a rated generator capacity up to three times larger than the capacity of the NREL 5 MW wind turbine considered in this study could be deployed in some of the floating wind projects planned towards 2026 [5]. Hence, it is important to consider how the wave periods

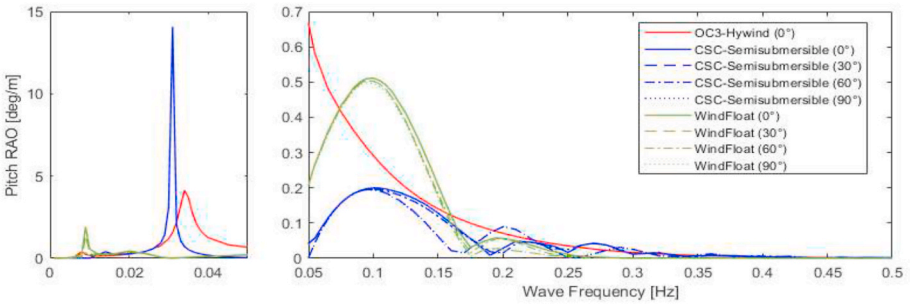

Fig. 15. Pitch motion RAOs at SWL along the wave heading direction for the OC3-Hywind (red), CSC-Semisubmersible (blue), and WindFloat (green).]. (For interpretation of the references to color in this figure legend, the reader is referred to the Web version of this article.)

resulting in horizontal wave loads in phase on the columns change with an upscaling of the floater. The scaling of the floater model does not generally scale linearly with the wind turbine, and a variation in floater model scale from 1.0 to 2.0 is considered in the following. The floater models that are analysed in this study corresponds to a scale 1.0.

Fig. 12 show how the wave periods leading to horizontal wave loads in phase on the different columns will change with different scaling for the CSC-Semisubmersible and WindFloat. It is seen that the wave periods will increase and that also even more periods will enter the wave period range when the scale is increased. When the wave periods increase from the lower end of the wave period range as shown in Fig. 12, the associated horizontal wave loads are expected to increase. A larger significant wave height will typically be associated with a higher spectral peak period; in addition the probability of occurrence of the sea state will typically increase. The latter is observed in the distributions in Figs. 4 and 5 for both the Norwegian and the South Korean locations considered in this study. In total, this indicates that the impact of horizontal wave loads in phase on the columns of semi-submersible FOWTs will increase with larger scale.

4.3. Comparison of RAOs relevant for human exposure

The pitch motion, as well as the lateral and vertical acceleration RAOs for the OC3-Hywind, CSC-Semisubmersible, and WindFloat are calculated along the dominant wave direction for several wave headings within the frequency range 0–0.5 Hz, respectively. The motions of the OC3-Hywind were found to be very little affected by the wave heading due to its symmetrical shape and negligible contribution from the catenary mooring system. For this reason, only results with 0° wave heading is presented for the OC3-Hywind.

A comparison of the lateral and vertical accelerations at the platform and the nacelle level are shown in terms relative to the gravitational acceleration, *g*, in Fig. 13 and Fig. 14 respectively. A comparison of the pitch motion at SWL is shown in Fig. 15. The following observations can be made from Figs. 13–15:

- The lateral accelerations at the nacelle level are approximately a factor ~2 larger than the accelerations at the platform level for OC3-Hywind and CSC-Semisubmersible while the vertical accelerations are almost unaffected by the vertical level for both concepts.
- The largest acceleration peak at ~0.19 Hz is lower at the nacelle level than at the platform level for WindFloat. This can be explained by the location of the centre of rotation above the nacelle level in this frequency range as shown in the left part of Fig. 11. There is also a shift in the peak frequency towards a lower frequency from the platform level to the nacelle level for WindFloat. The relative phase angle between surge and pitch in the right part of Fig. 11 show that surge and pitch are approximately 180° out of phase at the peak frequency for the platform acceleration, while they are approximately in phase at the peak frequency of approximately 0.17 Hz for the nacelle acceleration, and could explain the shift in peak frequency between the platform and nacelle levels. The vertical accelerations of WindFloat are larger at the nacelle level than the platform level for other wave headings than 0°, and the largest difference is observed for wave heading 60° with 49% increase in the peak acceleration RAO.
- The maximum peak values in the lateral nacelle acceleration RAOs within the wave frequency range (0.05–0.3 Hz) are quite similar among the three floater concepts, while the maximum peak value in the lateral platform acceleration RAOs is approximately a factor of 2 larger for WindFloat than for OC3-Hywind and CSC-Semisubmersible.
- The lateral accelerations of the CSC-Semisubmersible have significant variation with both wave heading and frequency. Different dominant peaks in the lateral accelerations are observed at certain wave headings at higher wave frequencies:
  - o The acceleration responses for 0 and 60° wave heading are very similar due to symmetry of the CSC-Semisubmersible floater. It is seen that the three dominant peaks at higher wave frequencies for these wave headings correspond with the wave frequencies with horizontal wave loading in phase in Table 3.
  - o The acceleration responses for 30 and 90° wave headings are also similar due to symmetry. The two dominant peaks at higher wave frequencies for these wave headings correspond with the wave frequencies with horizontal wave loading in phase in Table 3.
- The lateral accelerations of WindFloat have a similar variation with both wave heading and frequency as the CSC-Semisubmersible, and the dominant peaks in the platform lateral accelerations for WindFloat are in line with Table 4.

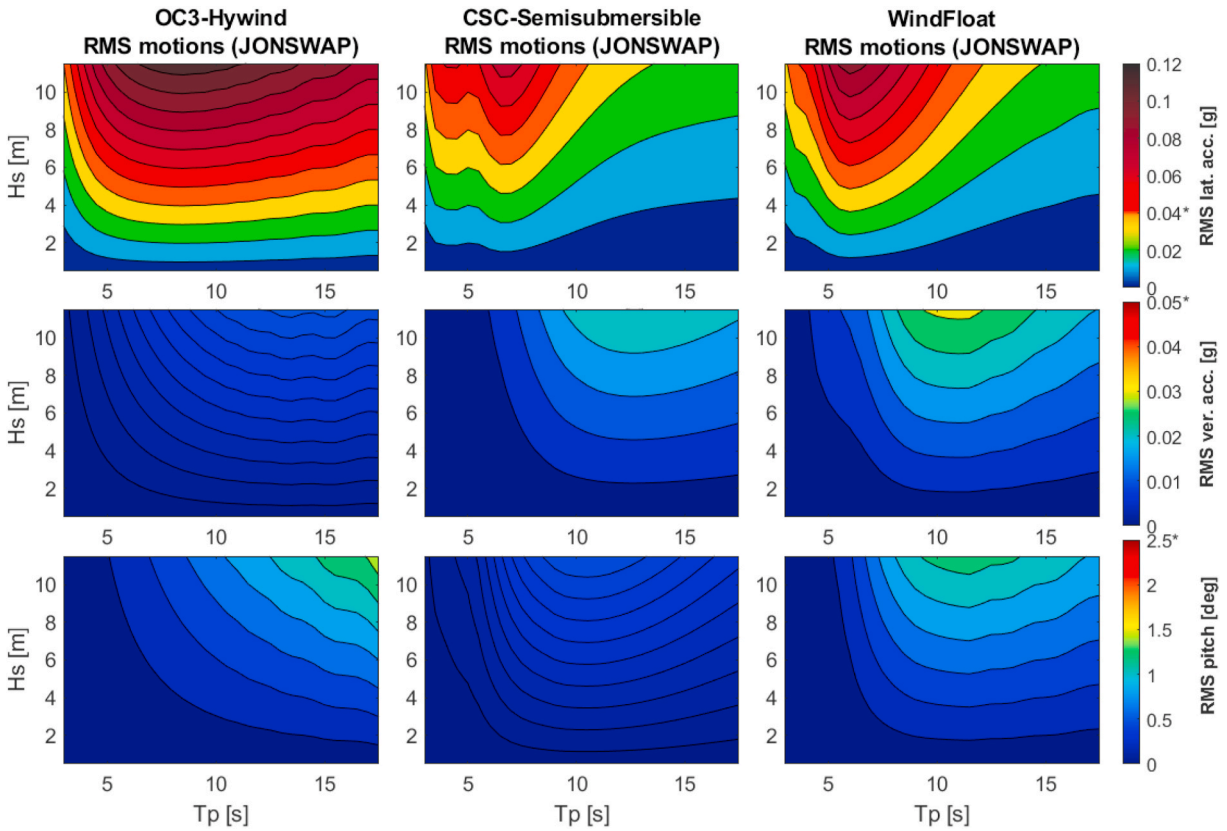

Fig. 16. *Nacelle level* response contour plots for the OC3-Hywind (left), CSC-Semisubmersible (middle) and WindFloat (right) from generic load cases using the JONSWAP wave spectrum with 0° wave heading. RMS values of lateral accelerations (top), vertical accelerations (middle), and pitch motion (bottom) at the *nacelle* level. The limiting RMS value is indicated with an asterisk (*) in the contour color axes on the right hand side. (For interpretation of the references to color in this figure legend, the reader is referred to the Web version of this article.)

- The pitch motion RAOs show that the CSC-Semisubmersible has approximately half the pitch response of WindFloat in the wave frequency range, while OC3-Hywind is within the response range of the two semisubmersible concepts.

5. Comparative simulation studies

5.1. Response contours from generic sea states

Generic RMS response contour plots for the relevant responses for motion sickness are developed by analysing the generic load case matrix with significant wave heights varying from 0 to 12 m and spectral peak periods varying from 3 to 17 s for the three FOWT concepts. Each sea state is analysed using both the JONSWAP and Torsethaugen wave spectra.

The response contour plots for the RMS values for the lateral and vertical accelerations, and the rotational motion, are shown for OC3-Hywind, CSC-Semisubmersible, and WindFloat in Fig. 16- Fig. 19. It is evident that it is only the limiting RMS criterion related to lateral accelerations (0.04 g) that can potentially be exceeded for any of the concepts considered. The limiting RMS criteria for vertical acceleration (0.05 g) and angular motion (2.5°) are not exceeded for any of the concepts, for any sea states, wave directions, or wave spectra considered. The focus in the following is therefore on the lateral accelerations.

Contour plots of the nacelle level lateral accelerations from analyses using the JONSWAP wave spectrum with 0° wave heading are shown in the upper part of Fig. 16. The contour plots for OC3-Hywind have a flat curve as function of spectral peak period, while both semisubmersible concepts have clear peaks and troughs that can be related to the acceleration RAOs in Fig. 12. Generally, OC3-Hywind has the highest nacelle acceleration level among the concepts, but WindFloat has a trough in the contour plot around 6 s to approximately the same level as OC3 Hywind. The CSC-Semisubmersible has the lowest nacelle acceleration level among the concepts.

The platform level lateral acceleration contour plots from analyses using the JONSWAP wave spectrum with 0° wave heading are shown in the upper part of Fig. 17. OC3-Hywind and the CSC-Semisubmersible has improved contours for the platform level compared to the nacelle level. However, the contours for WindFloat are worse at the platform level than at the nacelle level, with a deep trough for spectral peak periods around 5 s at the platform level. These findings are in line with acceleration RAOs in Fig. 12. It is also a clear indication that a person experiencing motion sickness should stay at the platform level onboard OC3-Hywind and CSC-

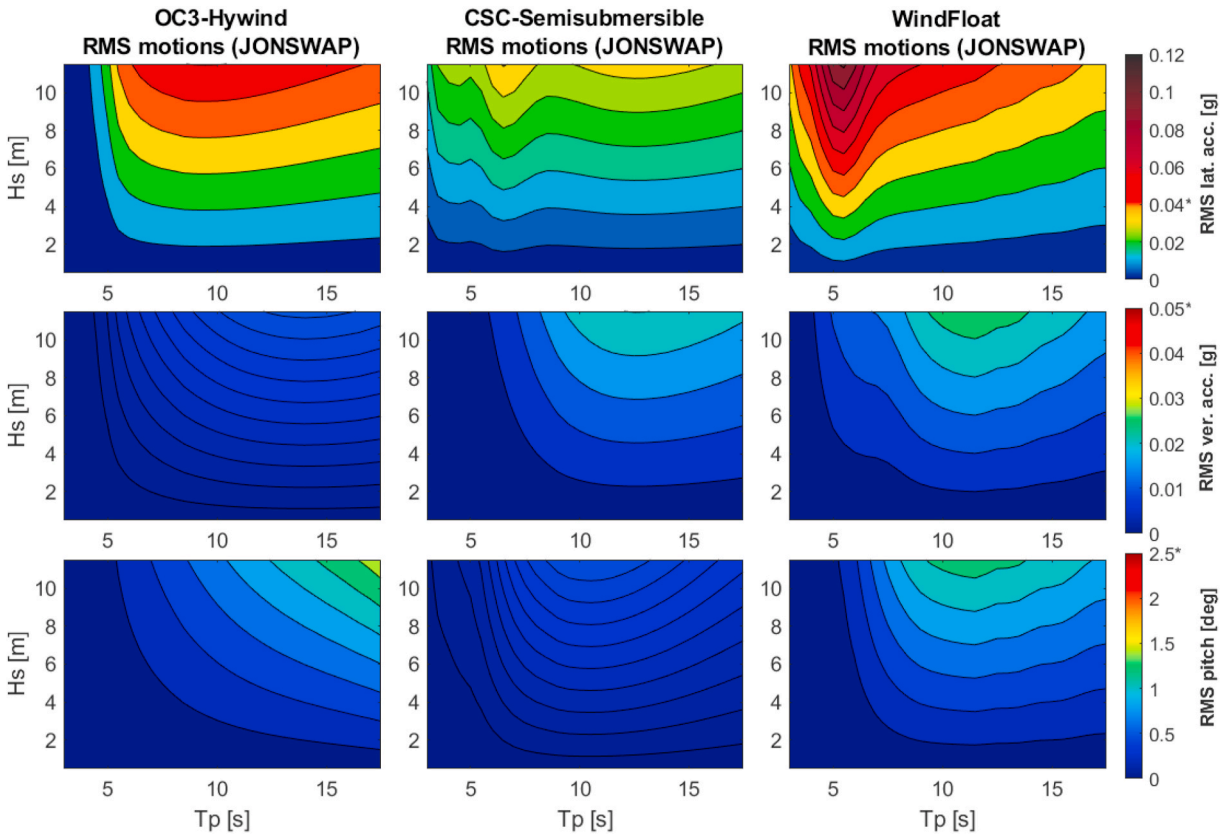

Fig. 17. *Platform level* response contour plots for the OC3-Hywind (left), CSC-Semisubmersible (middle) and WindFloat (right) from generic load cases using the JONSWAP wave spectrum with 0° wave heading. RMS values of lateral accelerations (top), vertical accelerations (middle), and pitch motion (bottom). The limiting RMS value is indicated with an asterisk (*) in the contour color axes on the right hand side. (For interpretation of the references to color in this figure legend, the reader is referred to the Web version of this article.)

Semisubmersible, and at the nacelle level onboard WindFloat.

Use of the double peaked Torsethaugen wave spectrum to generate the nacelle lateral acceleration contour plots for 0° wave heading are shown in the upper part of Fig. 18. The lateral acceleration contours are found to be less curved compared to the corresponding contours using the JONSWAP wave spectrum in Fig. 16:

The contours for OC3 Hywind has increased accelerations at low wave periods due to contribution from the low frequency peak in the double-peaked Torsethaugen wave spectrum. On the other hand, the accelerations at the trough spectral peak period is reduced due to the contribution from the high frequency peak in the Torsethaugen wave spectrum.

- The lateral acceleration contours for both semisubmersible floaters are both reduced and less curved since the energy content at the relatively narrow troughs in spectral peak period range will be reduced when using a double peaked wave spectrum.

The effect of a wave heading of 30° on the nacelle lateral accelerations from analyses using the JONSWAP wave spectrum are shown for CSC-Semisubmersible and WindFloat in the upper part of the contour plots in Fig. 19:

- The contours for the CSC-Semisubmersible have changed from having two troughs at 0° wave heading to having one trough at 30° wave heading. The acceleration level at the single trough is about the same level as at the largest trough for 0° wave heading. The frequency of the trough is shifted to between the two troughs at 0° wave heading. This is in line with the nacelle lateral acceleration RAOs in Fig. 13.
- The nacelle acceleration contour for WindFloat is significantly improved for 30° wave heading and WindFloat has smallest nacelle lateral accelerations among the concept for this wave heading. This is also in line with the nacelle lateral acceleration RAOs in Fig. 13.

5.2. Calculation of workability index for two specific locations

The workability index from Equation (5) is calculated for several threshold levels for the significant wave height for OC3-Hywind,

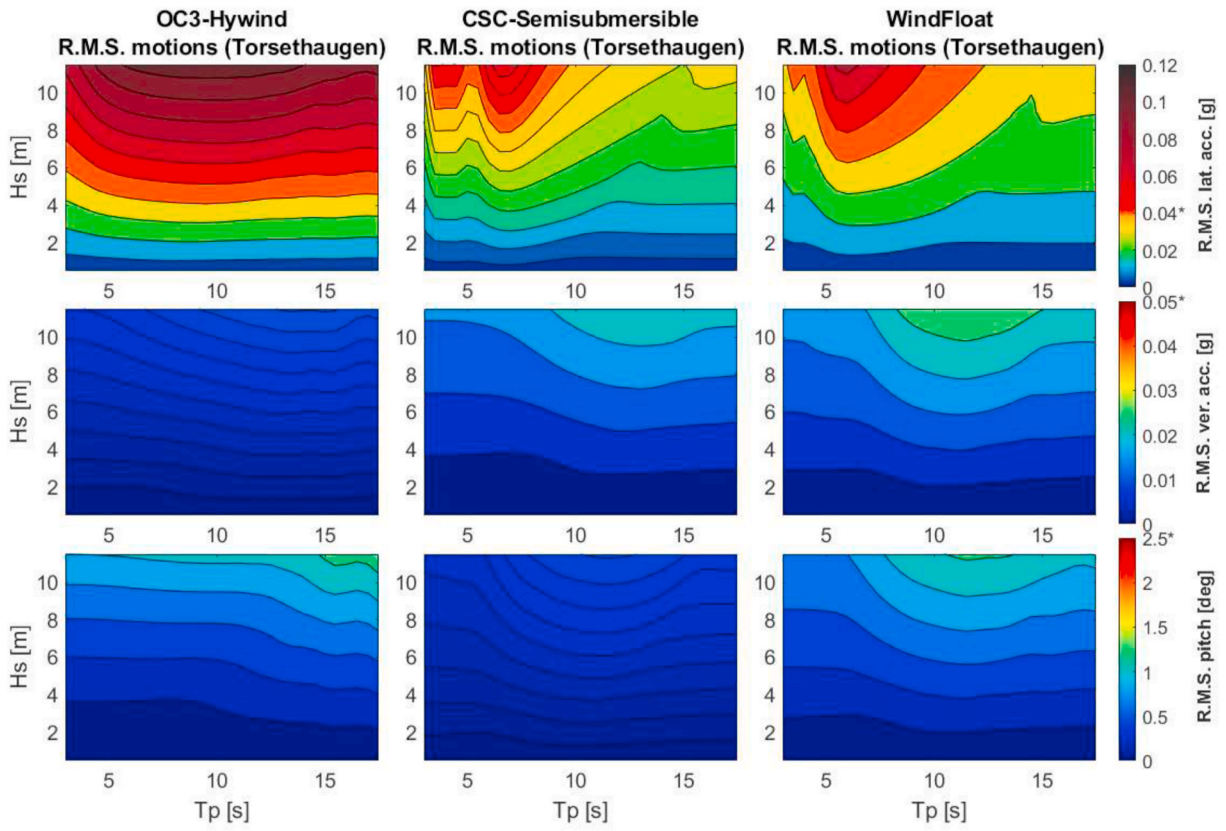

Fig. 18. *Nacelle level* response contour plots for the OC3-Hywind (left), CSC-Semisubmersible (middle) and WindFloat (right) from generic load cases using the Torsethaugen wave spectrum with 0° wave heading. RMS values of lateral accelerations (top), vertical accelerations (middle), and pitch motion (bottom) at the *nacelle* level. The limiting RMS value is indicated with an asterisk (*) in the contour color axes on the right hand side. (For interpretation of the references to color in this figure legend, the reader is referred to the Web version of this article.)

CSC-Semisubmersible, and WindFloat for two locations relevant for floating wind deployment. One location is at the coast of Norway and the other location is at the coast of South Korea, and the reduced metocean data sets from Fig. 4 are applied in the analyses.

The operational limit related to the significant wave height is strongly dependent on the type of vessel used for crew transfers. CTVs vary from 1.5 to 2.5 m in operational limit, while conventional SOVs with 8–10 times higher daily rate can operate in harsher sea conditions with significant wave height up to 4.5–5.0 m [6].

The workability index of the three FOWT concepts are shown as function of limiting significant wave height for both locations in Fig. 20 and Fig. 21. The workability index for work on the platform level is shown in Fig. 19. The workability index for the platform level is 1 for significant wave heights up to 5 m regardless of concept, location, and wave spectrum used in the analyses.

The workability index for work on the nacelle level is shown in Fig. 21. The workability index for the nacelle level is 1 for significant wave heights up to 3.5 m regardless of concept, location, and wave spectrum used in the analyses. The significant wave height of 3.5 m corresponds to the maximum significant wave height for crew transfers to FOWTs reported in Ref. [8]. Both semisubmersible concepts have a workability index of 1 even for significant wave heights up to 5 m. OC3-Hywind has a reduction in workability index for significant wave heights above 3.5 m due to exceedance of the limiting RMS criteria on lateral accelerations (0.04 g):

- The reduction in workability index is largest when using the JONSWAP wave spectrum at both locations, which is in correspondence with the lateral acceleration contour plots in Figs. 16 and 18.
- The reduction in workability index is significantly larger at the Norwegian location compared to the South Korean location. This is probably due to the higher probability of low spectral peak periods at the South Korean location as indicated in Fig. 5, combined with the lateral acceleration contours in Figs. 16 and 18 showing lower lateral accelerations for low spectral peak periods for OC3-Hywind.

6. Conclusions

Three well-defined 5 MW floating wind concepts, i.e., OC3-Hywind (spar buoy), CSC Semi-submersible (semi-submersible) and WindFloat (semi-submersible), have been analysed with respect to human exposure to motion during maintenance operations. The

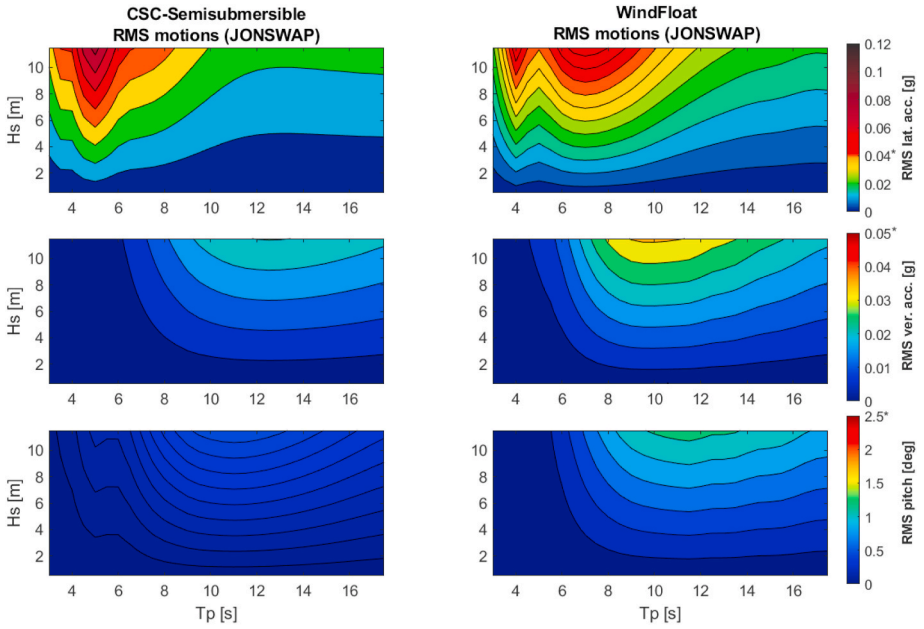

Fig. 19. *Nacelle level* response contour plots for the CSC-Semisubmersible (left) and WindFloat (right) using the JONSWAP wave spectrum with 30° wave heading. RMS values of lateral accelerations (top), vertical accelerations (middle), and pitch motion (bottom). The limiting RMS value is indicated with an asterisk (*) in the contour color axes on the right hand side. (For interpretation of the references to color in this figure legend, the reader is referred to the Web version of this article.)

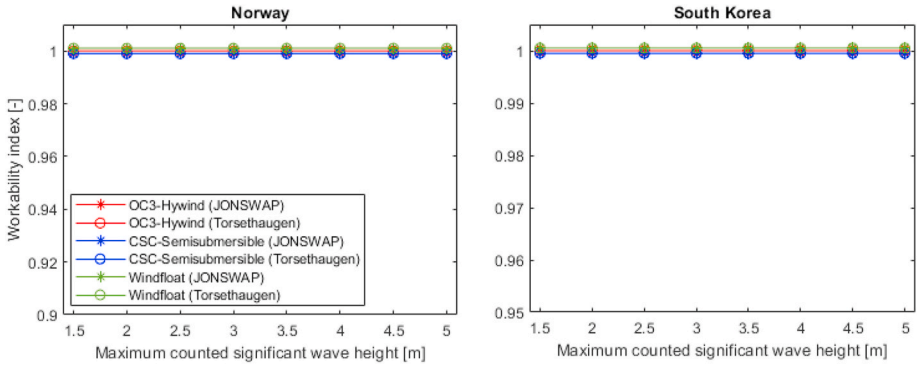

Fig. 20. *Platform level* workability index for OC3-Hywind (red), CSC-Semisubmersible (blue), and WindFloat (green) using the JONSWAP (circle) and Torsethaugen (asterisk) wave spectra for a location in Norway (left) and South Korea (right). (For interpretation of the references to color in this figure legend, the reader is referred to the Web version of this article.)

relevant motion response criteria are based on root mean square values of lateral and vertical accelerations, and pitch motions.

The three floating wind concepts exhibit very different motion characteristics although their natural periods are not very different. Dynamic properties of the concepts such as the vertical position of the centre of rotation, the phase angle between surge and pitch motion, and wavelengths corresponding to horizontal loading in phase or 180° out of phase on the different columns of the floaters for different wave directions can to a large extent describe the observed characteristics.

The effect of upscaling of the 5 MW semisubmersible concepts are investigated with respect to horizontal wave loads in phase on the different columns. When the scale is increased the wave periods leading to horizontal wave loads in phase on the columns will increase, and also more wave periods will enter the wave period range above 3 s. In total, this indicate that the impact of horizontal wave loads in phase on the columns of semi-submersible FOWTs will increase with scale.

Contour response plots of the relevant motion response criteria for work at the nacelle level and at the platform level are calculated for a generic load case matrix for a range of relevant spectral peak periods and significant wave heights using both the single peaked JONSWAP and the double peaked Torsethaugen wave spectra. The main findings from the response contour plots are:

- Only the lateral acceleration limit can potentially be exceeded for the three floating wind concepts considered.

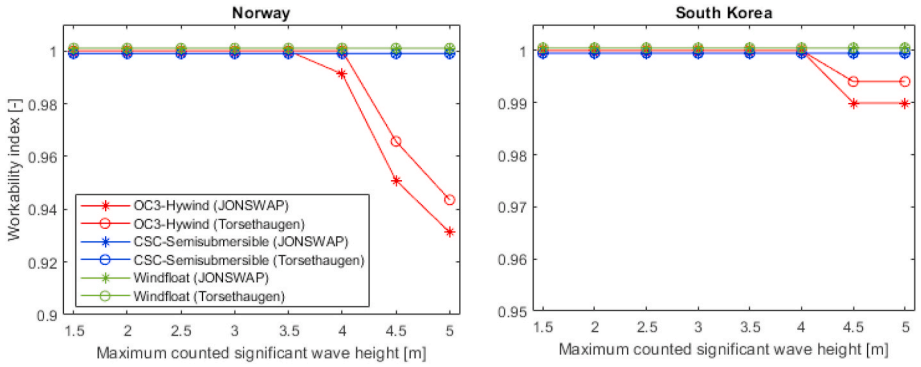

Fig. 21. *Nacelle level* workability index for OC3-Hywind (red), CSC-Semisubmersible (blue), and WindFloat (green) using the JONSWAP (circle) and Torsethaugen (asterisk) wave spectra for a location in Norway (left) and South Korea (right). (For interpretation of the references to color in this figure legend, the reader is referred to the Web version of this article.)

- The lateral accelerations are generally reduced when using the double peaked Torsethaugen wave spectrum compared to using the single peaked JONSWAP spectrum.
- The lateral acceleration contour for OC3-Hywind has a quite flat curve as function of spectral peak period, while both semi-submersible concepts exhibits several peaks and troughs that typically corresponds with wavelengths with horizontal loading in or out of phase on the columns.
- The lateral accelerations of OC3-Hywind and CSC-Semisubmersible are significantly larger at the nacelle level than on the platform level, while the observation is opposite with WindFloat, partly due to a high centre of rotation above the nacelle level in an important frequency range. This implies that a person exposed to motion sickness onboard OC3-Hywind or CSC-Semi-submersible should seek refuge towards the platform level to recover, while a person onboard WindFloat should seek refuge towards the nacelle level.
- Overall, the CSC-semisubmersible has the lowest lateral acceleration level at the platform and nacelle levels, but the lateral accelerations at the nacelle level for WindFloat are smallest among the concepts for wave headings from 30° (and 90, 150, 210, 270°) due to wave loading out of phase on the columns for wavelengths corresponding to the horizontal distance between the columns.

The concept of a workability index is utilised to present the performance of the different floating wind concepts with respect to exposure of maintenance personnel to motion. The workability indices for the three floating wind concepts are calculated for the nacelle and platform levels using both the JONSWAP and Torsethaugen wave spectra for two locations relevant for floating wind deployment. A reduced set of load cases (~500 cases) have been selected with a good representation of the distributions for significant wave height, spectral peak period, and wave heading for the coasts of Norway and South Korea. The main finding is that the workability index is equal to 1, for both the platform and nacelle level, regardless of concept, location, and wave spectrum used in the analyses, for significant wave heights up to 3.5 m which corresponds to the maximum significant wave height for crew transfers to FOWTs.

Declaration of competing interest

The authors declare that they have no known competing financial interests or personal relationships that could have appeared to influence the work reported in this paper.

Acknowledgement

The authors would like to thank Equinor ASA for providing hindcast data for two relevant locations for future floating wind deployment in Norway and South Korea.

References

[1] Musial W. “NREL,”. https://www.nrel.gov/news/program/2020/floating-offshore-wind-rises.html; 2 April 2020.
[2] Hopstad A, Ronold K, Slätte J. “Design standard for floating wind turbine structures,”. In: 10th deep sea offshore wind R&D conference; 2013. Trondheim.
[3] Skaare B, Nielsen F, Hanson T, Yttervik R, Havmøller O, Rekdal A. Analysis and measurements from the Hywind Demo floating wind turbine. ” *Wind Energy*; 2015.
[4] Roddier D, Cermelli C, Aubault A, Peiffer A. Summary and conclusions of the full life-cycle of the WindFloat FOWT prototype project. In: International conference on offshore mechanics and arctic engineering. Trondheim, Norway.; 2017.
[5] QFWE. Global Floating Wind. In: Market and Forecast Report. 2021–2034. ” Quest Floating Wind Energy; 2021.
[6] Hu B, Stumpf P, van der Dejil W. Annual offshore wind access Report. ” TNO; 2019.
[7] 4COffshore. “4coffshore,” 4C offshore. https://www.4coffshore.com/support/an-introduction-to-crew-transfer-vessels-aid2.html; 2021.

[8] Scheu M, Matha D, Schwarzkopf M-A, Kolios A. Human exposure to motion during maintenance on floating offshore wind turbines. Ocean Eng 2018;165:293–306.
[9] Gomes HM, Savionek D. Measurement and evaluation of human exposure to vibration transmitted to hand-arm system during leisure cyclist activity. Brazilian J Biomed Eng 2014;4(30):291–300.
[10] Mansfield NJ. Human response to vibration. New York: CRC Press; 2005.
[11] NORDFORSK. The nordic cooperative project, seakeeping performance of ships assessment of a ship's performance in a seaway. Trondheim: Marintek; 1987.
[12] Hasselmann K, Barnett T, Bouws E, Carlson H, Cartwright D, Enke K, Ewing J, Gienapp H, Hasselmann D, Kruseman P, Meerburg A, Müller P, Olbers D, Richter KSW, Walden H. Measurements of wind-wave growth and swell decay during the Joint North Sea Wave project (JONSWAP). Dtsch Hydrogr Z 1973;12.
[13] Torsethaugen K, Haver S. Simplified double peak spectral model for ocean waves. Touson: *ISOPE*; 2004.
[14] Guanche R, Martini M, Jurado A, Losada IJ. Walk-to-work accessibility assessment for floating offshore wind turbines. Ocean Eng 2016:216–25.
[15] Wolfram J. On alternative approaches to linearization and Morison's equation for wave forces. Proceedings of the Royal Society of London. Series A: Mathematical, Physical and Engineering Sciences; 1988.
[16] DNV. GeniEUser manualvol. 1. Concept design and analyses of offshore structures; 2016.
[17] DNV. Wadam user manual. Wave analysis by diffraction and Morison theory; 2014.
[18] DNV GL. DNVGL-CG-0130. DNV GL; 2018.
[19] DNV GL. DNV-RP-C205. Det Norske Veritas; 2010.
[20] DNV GL. DNV-RP-H103. Det Norske Veritas; 2011.
[21] Çakıcı F, Yıldız B, Alkan AD. Crew comfort investigation for vertical and lateral responses of a container ship. In: 12th international Conference on the Stability of Ships and ocean vehicles; 2015. Glasgow.
[22] Dolinskaya IS, Kotinis M, Parsons MG, Smith RL. Optimal short-range routing of vessels in a seaway. J Ship Res 2009;53(3):121–9.
[23] Payne PR. On quantizing ride comfort and allowable accelerations. In: AIAA/SNAME advanced marine vehicles conference; 1976.
[24] International Organization for Standardization. ISO 2631/3. Geneva: ISO; 1985.
[25] Jonkman J, Butterfield S, Musial W, Scott G. Definition of a 5-MW reference wind turbine for offshore system development. " National Renewable Energy Laboratory; 2009.
[26] Jonkman J. Definition of the floating system for phase IV of OC3. " National Renewable Energy Laboratory; 2010.
[27] Luan C, Gao Z, Moan T. Design and analysis of a braceless steel 5-mw semi-submersible wind turbine. In: 35th international Conference on ocean. Busan: Offshore and Arctic Engineering; 2016.
[28] Roddier D, Peiffer A, Aubault A, Weinstein J. A generic 5 MW WindFloat for numerical tool validation & comparison against a generic spar. In: Proceedings of the ASME 2011 30th international Conference on ocean. Rotterdam: Offshore and Arctic Engineering; 2011.
[29] Luan C, Chabaud V, Bachynski EE, Gao Z, Moan T. Experimental validation of a time-domain approach for determining sectional loads in a floating wind turbine hull subjected to moderate waves. In: 14th deep sea offshore wind R&D conference. Trondheim: EERA DeepWind; 2017. 2017.
[30] Skaare B, Hanson TD, Nielsen F, Yttervik R, Hansen A, Thomsen K, Larsen T. "Integrated dynamic analysis of floating offshore wind turbines," in *EWEC 2007*. Milano: European Wind Energy Conference & Exhibition; 2007.
[31] Faltinsen OM. Sea loads on ships and ocean structures. Cambridge: Cambridge University Press; 1990.